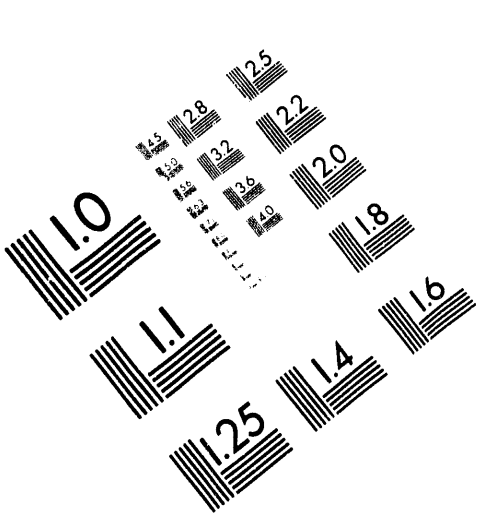

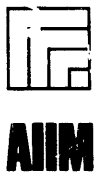

Association for Information and Image Management

1100 Wayne Avenue, Suite 1100
Silver Spring, Maryland 20910

301/587-8202

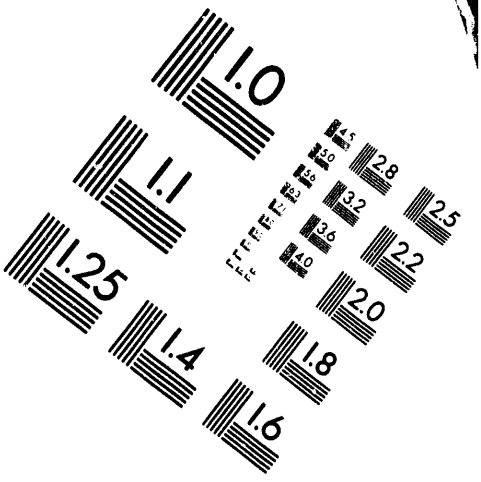

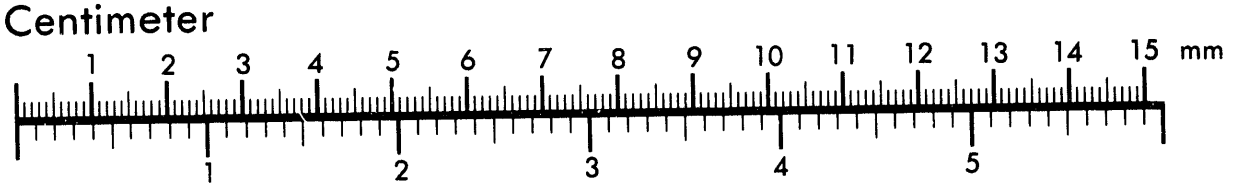

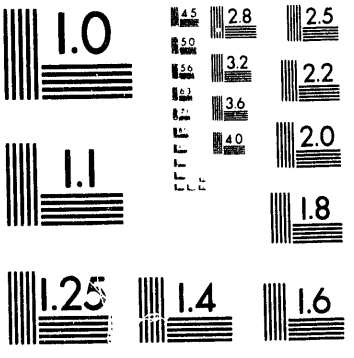

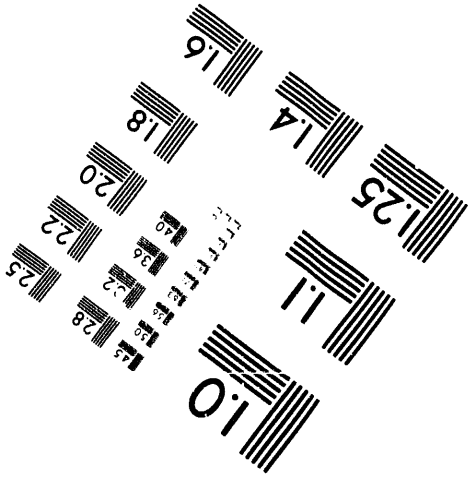

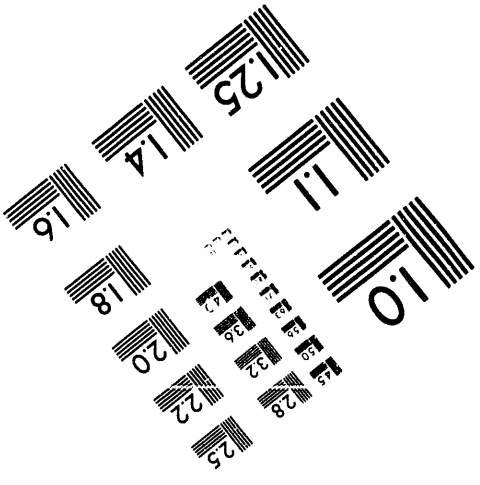

1 of 1

2

Conf-9304144--10

UCRL-JC-113165
PREPRINT

Time-Resolved Probing of Electron Thermal Conduction in Femtosecond-Laser-Pulse-Produced Plasmas

B.-T.V. Vue
A. Szoke
O.L. Landen

This paper was prepared for submittal to the
Second International Conference on Laser Ablation
Knoxville, Tennessee
April 19-22, 1993

June 1993

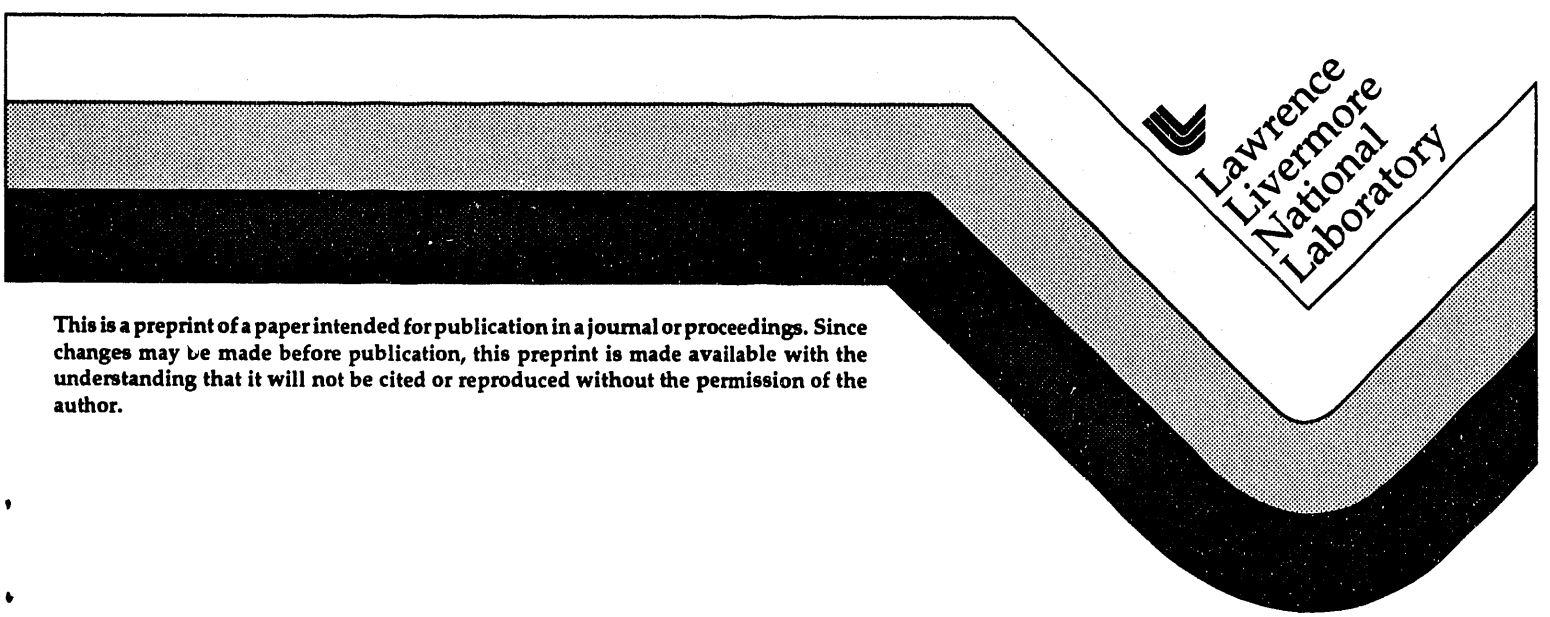

Time-Resolved Probing of Electron Thermal Conduction in Femtosecond-Laser-Pulse-Produced Plasma

B.-T. V. Vu*, A. Szoke, and O. L. Landen
Lawrence Livermore National Laboratory, Livermore, CA 94550
**and with Dept. of Applied Science, U.C.D., Livermore, CA 94550*

ABSTRACT

We present time-resolved measurements of reflectivity, transmissivity and frequency shifts of probe light interacting with the rear of a disk-like plasma produced by irradiation of a transparent solid target with 0.1ps FWHM laser pulses at peak intensity $5x10^{14}W/cm^2$. Experimental results show a large increase in reflection, revealing rapid formation of a steep gradient and overdense surface plasma layer during the first picosecond after irradiation. Frequency shifts due to a moving ionization created by thermal conduction into the solid target are recorded. Calculations using a nonlinear thermal heat wave model show good agreement with the measured frequency shifts, further confirming the strong thermal transport effect.

INTRODUCTION

Recent developments in the generation of high power femtosecond laser pulses offer new possibilities in the studies of ultrafast phenomena that are unresolved in the past. For example, time-resolved reflectivity, transmissivity and frequency shift measurements of the probe light interacting with laser-produced plasmas provide time-resolved information on laser absorption, plasma formation and energy transport mechanisms.[1,2] Particularly, in irradiation of a solid target with a high intensity ($>10^{12}W/cm^2$) and ultrashort ($<10^{-12}s$) laser pulse, a high temperature and solid density plasma layer is quickly formed at the target surface during the rising edge of the laser pulse.[1] As a result, the remainder of the laser pulse is shielded from the bulk region behind the critical density surface ($3x10^{21}/cm^3$) where the plasma frequency is greater than the laser frequency. The remainder of the pulse however continues to interact with the surface plasma and deposit its energy at and above the critical density.[3] The energy thus absorbed at the surface is then transported into the bulk region via electron thermal conduction super-sonically until expansion of the surface plasma becomes important and the resultant rarefaction shock wave overtakes the thermal wave.[4,5]

In this paper we report high temporal resolution (~0.1ps) probing of the electron thermal transport in a plasma produced by pump laser irradiation of a transparent target. Measurements of reflectivity, transmissivity and frequency shifts of a probe pulse are recorded as functions of the relative time delay between the pump and probe pulse. The probe pulse interacting with the plasma at the frontside (vacuum-surface side) determine characteristic time scales for formation of the overdense plasma layer at the surface and its subsequent expansion into the surrounding vacuum. The backside probe pulse light, on the other hand, interacts with a thermal wave supported by electron conduction into the solid target. Frontside and

backside probing allows us to encompass the totality of the plasma evolution and provides different but complementary information about energy transport mechanisms.

EXPERIMENTAL RESULTS & CALCULATIONS

A similar detailed schematic of the pump-probe experiment has been described elsewhere.[1] The laser system[6] now includes a colliding pulse, mode locked ring oscillator producing low energy 0.1ps pulses at a center wavelength λ = 616nm and a repetition rate of 90MHz. The pulses are selected for amplification at 10Hz in a series of a six-pass bowtie amplifier and two Bethune amplifiers. The 2mJ, 0.1ps amplified pulses are then directed into a vacuum spatial filter to improve beam transverse mode quality and focusability, and are split into a strong pump and a weaker probe pulse. The pump pulse is normally incident onto the front surface of a target with a peak intensity of $5 \times 10^{14} W/cm^2$ and a focal spot of 75μm in diameter. The probe pulse focal spot is 25μm with an intensity of $2 \times 10^{10} W/cm^2$, sufficiently low to be non-intrusive but still sufficiently high to discriminate the probe specular reflection from the diffusely scattered light of the intense pump pulse. Polarization of the probe is S-polarized, orthogonal to that of the pump, so that diffuse light of the pump may be rejected before detection. Energies of the incident, reflected and transmitted probe are simultaneously monitored by P.I.N. diodes. When the probe is redirected to probe the plasma from the backside at 30° to the normal at the rear surface of the target, the corresponding internal incident angle is θ =19°, fixing the interaction length at ≈100μm between the pump and the backside probe paths. In addition to reflectivity and transmissivity measurements, the backside probe pulse reflection can also be sent to a grating spectrometer (0.33m, 1200 lines/mm) coupled to a multichannel analyzer (0.4Å/pixel). The transparent fused quartz target is 1.6mm thick and is coated with an amorphous carbon thin (300Å) film at the front surface. The target is also coated with an anti-reflection film on its rear surface to suppress probe light reflection from that surface. The measured cold carbon film absorptivity, reflectivity and transmissivity are 15%, 7% and 78%, respectively. The highly absorptive film at the surface promotes large laser absorption and confines most of energy deposition to the surface, thus setting up a high temperature heat source for subsequent generation and propagation of a thermal wave supported by electron conduction into the bulk transparent region. The carbon film also eliminates effects of induced phase modulation[7] and formation of an underdense bulk plasma by lowering the threshold for critical surface plasma formation, hence attenuating the transmitted pump pulse energy.[1] The target is mounted on a computer-driven translation stage so that on each shot the laser fires on a fresh part of the target while the overlap conditions of the two beams are maintained.

Fig.1a shows simultaneous scans of the frontside probe reflection and transmission as function of time delay between the pump and the probe pulses. Zero-time delay is estimated to within ±0.05ps by comparison with picosecond experiments.[1,7] The single shot data has been divided by the incident energy and normalized to the absolute values of the cold target. In both data scans, the plateaus during early or negative delay correspond to the values for the undisturbed target where the probe arrives prior to the pump. At some later delay when an overdense or super-critical plasma layer is formed at the surface during the onset of the pump pulse, the probe transmission decreases to zero. At the same time, the pump pulse

continues to deposit its energy at the surface plasma. As a result, the surface plasma becomes hotter, denser and highly reflective like that of metallic mirror,[8] resulting in an increase in the probe reflection. The 10-90% risetime of the reflection enhancement is about 1ps longer than the decay time of the transmission data. Following the increase, the probe reflection experiences a slow decay which is due to increasing absorption by the underdense or sub-critical plasma region as the overdense surface plasma expands and cools. The 1/e falltime for the reflection is ≈6ps. Fig.1b displays the reflection and transmission data for the backside probe beam. The data again shows a drop in transmission and increase in reflection due to the formation of a super-critical surface plasma. The reflection increase however is followed by a much slower decay time of 15ps than for the frontside probe reflection data. The backside reflection enhancement shows that the plasma as seen from the rear side also acts as a highly reflective mirror, indicating a steep density gradient at high density and temperature.

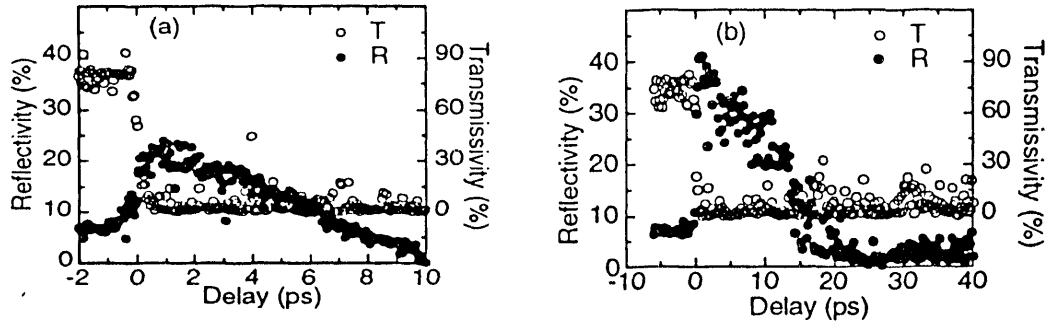

FIG.1: Simultaneous scans of single-shot reflection (close circles) and transmission (open circles) of (a) the frontside probe and (b) backside probe pulses are measured as functions of time delay between the strong pump and weak probe pulses.

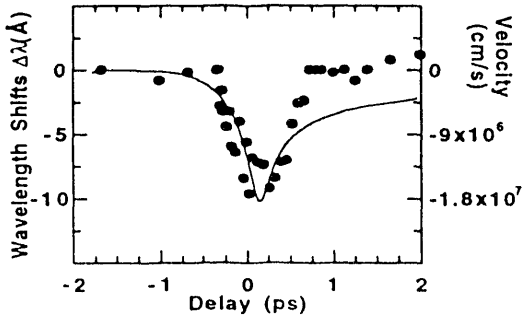

FIG.2: Wavelength shifts (close circles) in the enhanced reflected backside probe light are observed during the first picosecond after the pump pulse. Solid curve is calculated shifts from the nonlinear heat wave model.

In Fig.2 the wavelength shifts $\Delta\lambda$ (solid dots) of the center-of-gravity wavelength component in the spectrum of the reflected backside probe are shown as a function of delay. Each data point is an average of 90 laser shots and has a statistical uncertainty of ±0.8Å. The shifts $\Delta\lambda$ are proportional to the velocity v of the thermal wave or ionization front and are determined by the Doppler formula:

$$\frac{\Delta\lambda}{\lambda} = -2n_o \cos\theta \frac{v}{c} \qquad (1)$$

The factor of 2 accounts for reflection, $\theta = 19°$, $n_0 = 1.46$ is the solid target refractive index, c is the speed of light. The observed maximum shift of 10Å corresponds to a maximum velocity of 1.8×10^7cm/s. This is at least about 4 times greater than the maximum ion sound velocity of the plasma as was inferred from the measured maximum frequency shifts of 7Å in the frontside probe light and calculations using the model for a isothermally expanding plasma.[9] Hence this ionization front is supersonic and is attributed to a thermal wave.

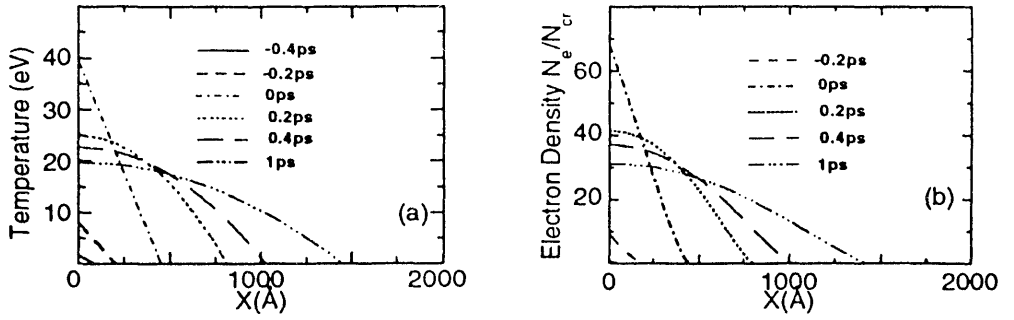

FIG.3: (a) Calculated electron temperature profiles at different instants as predicted by the nonlinear heat wave model. The simple approximate method to the Saha equations [10] is used to estimate (b) the corresponding electron plasma density profiles in the bulk target.

We now calculate the temperature and electron density evolution in the carbon-coated transparent target during the first few picoseconds. The electron temperature profile T_e and density N_e are approximately given the nonlinear heat diffusion equation for the electrons (in cgs units) :

$$\frac{\partial}{\partial t}\left[\frac{3}{2}N_e T_e + \frac{1}{3}\left(2\sum_{z=1}^{8} N_z \chi_z + \sum_{z=1}^{14} N_z \chi_z\right)\right] = \frac{\partial}{\partial x}\left(k_e \frac{\partial}{\partial x} T_e\right) \qquad (2)$$

Here N_z is the density of ions of charge +Z. The first term is electron thermal energy, and the second and third terms are energies stored in the plasma ionization states of oxygen and silicon ions, respectively. The term in the right hand side is the electron energy flux with Spitzer thermal conductivity[11] $k_e \approx 2.5 \times 10^{-4} T_e^{5/2} / Z_{eff}$. The left boundary condition to the equation is taken to be[12] $T_e(0,t) = T_o e^{2\gamma t}$ for $t \le 0$, and $\partial T_e(0,t) / \partial x = 0$ for $t > 0$. The right boundary condition is $T_e(+\infty, t) = 0$. T_o is determined by the total absorbed energy. A pump energy absorption of approximately 56% is inferred from the 36% specular reflection and 8% transmission of the pump pulse. The level of diffusely scattered light of the pump pulse has been measured by others [8,13] and is small (<5%) because during the pump pulse there is very little plasma expansion and the target surface remains optically flat. After the heating ($t > 0$) there is no heat flux at the surface as described by the left boundary condition for $t > 0$. With these conditions the solution to eqn.(2) for $t < 0$ is similar to that of the

Marshak radiation wave [14] and for t >0 the same as that of Zeldovich[15]. In the equation we have ignored plasma expansion because of its long characteristic time as was shown in the frontside probe data (Fig.1a). Also, we have performed the same backside probe reflection and transmission measurements with glass targets containing 27% impurities of readily-ionized materials[16] and found that the reflection decay time of 1ps is 15 times faster. Because energies of x-ray photons emitted from the surface plasma (~40eV) is much greater than the band gap energies (8-9eV) between the valence and conduction bands for both targets and easily excites the valence electrons into the conduction bands; had the x-ray contribution been dominant, we would have expected no significant difference in the reflection data for both targets. Thus, x-ray preheating of the cold region is negligible, if any significance. This is as expected since total Bremsstrahlung emission accounts for less than 1% of the plasma energy;[17] and the total thermal radiation emitted from the surface plasma is negligibly small ($\approx 5 \times 10^8 W/cm^2$). Electron density at a given temperature is obtained by using the Saha equation[10] The use of the Saha equation may not be completely valid. However, because collisional rates dominate over the radiative processes, the electron-electron equilization time is <1fs which quickly results in a Maxwellian electron distribution, and high stage ionization rates are small for temperatue <100eV, the Saha equation should be a good approximation. Fig.3a displays calculated snapshots of the temperature distribution at different instants. The surface temperature from room temperature rises as rapidly as the laser pulse, $\gamma = 10^{13}/s$. At the same time, the thermal wave front moves inward supersonically. For t > 0, the surface temperature relaxes gradually and the thermal wave slows down as the diffusion of the absorbed energy continues further into the colder region. Fig.3b shows the evolution of electron density normalized to the critical density ($\approx 3 \times 10^{21}/cm^3$). As is expected, during the pump pulse the super-critical surface plasma becomes progressively denser and thicker as a result of thermal transport, making the plasma more reflective as was observed. At later time, the plasma cools and its scale length in the bulk region below the critical level increases, leading to increasing absorption of the probe light. Thus, at late delay there is a competition between the highly reflecting overdense surface plasma and the increasing absorption by the underdense region, resulting in the observed long decay in the backside probe reflection. Further detailed calculations of both frontside and backside reflectivity, transmissivity by the Helmholtz equation will be given in future publication. The critical density velocity of the moving mirror-like plasma surface varies as a function of time, and thus different portions of the probe pulse suffer different amounts of blue shifts. Fig.2 also displays the calculated profile (solid curve) of the critical density velocity or wavelength shifts convolved over the finite probe pulse, showing fairly good agreement with the experimental results. The discrepancy in the data at late delay $t_d \geq 0.7$ps suggests some inhibition of the thermal transport and is probably attributed to the combined effect of the thermal transport and appearance of a rarefaction wave as plasma expansion becomes significant.[18]

CONCLUSION

In conclusion we have presented experimental results from both frontside and backside probing of a plasma produced by high intensity ultrashort laser pulse irradiation of a transparent target. The frontside probe data determines the characteristic time constants for rapid formation and subsequent expansion of the

super-critical surface plasma. The plasma as seen from the backside has a steep gradient as indicated by the reflection enhancement. The measured backside probe frequency shifts further confirms a highly reflective supersonic ionization front which is suggestive of a supersonic thermal wave supported by electron conduction. This together with the good fit by calculations using the nolinear heat wave model suggests electron conduction is as important as the most effective energy transport mechanism into the solid during the first picosecond after laser irradiation. Furthermore, the backside probe data has demonstrated we can successfully isolate thermal transport effects.

We gratefully acknowledge A. Hazi and R. Bauer for their strong support of the project. We also wish to thank M. Eckart, R. Stewart and D. Price for providing us laser time and some experimental apparatus. This work was performed under the auspices of U. S. Dept. of Energy by Lawrence Livermore National Laboratory under contract No. W-7405-ENG-48.

REFERENCES

1. B.-T. V. Vu, O. L. Landen & A. Szoke. "*Time-resolved backside optical probing of picosecond-laser-pulse-produced plasma in solid materials*", accepted for publication, Phys. Rev. E (1993).
2. X. Y. Wang & M. C. Downer. Opt. Lett. 17, 1450 (1992).
3. G. J. Tallents & et al. Phys. Rev. A 40, 2857-2859 (1989).
4. S. I. Anisimov. Sov. Phys. JETP 31, 181-182 (1970).
5. W. Rozmus & V. T. Tikhonchuk. Phys. Rev. A 42, 7401 (1990).
6. W. E. White, H. Nathel, W. Tulloch & D. M. Gold. *A Compact laser system for producing sub-100fs laser pulses with millijoule energies* (Presented at APS Meeting, Cincinnati, Ohio, 1990).
7. B.-T. V. Vu, A. Szoke & O. L. Landen. *"Induced-frequency shifts by counter-propagating subpicosecond optical pulses"* , accepted for publication, Opt. Lett. (1993).
8. M. M. Murnane, H. C. Kapteyn & R. C. Falcone. Phys. Rev. Lett. 62, 155 (1989).
9. O. L. Landen & W. E. Alley. Phys. Rev. A 46, 5089 (1992).
10. Y. P. Raizer. Sov. Phys. JETP 9, 1124 (1959).
11. L. Spitzer. *Physics of Fully Ionized Gases* (Interscience Publisher, New York, 1956).
12. J. F. Ready. J. Appl. Phys. 36, 462 (1965).
13. R. Fedosejevs *et al.* Phys. Rev. Lett. 64, 1250 (1990).
14. R. E. Marshak. Phys. Fluids 1, 24 (1958).
15. Y. B. Zeldovich & Y. P. Raizer. *Physics of ShocK Waves & High Temperature Hydrodynamic Phenomena* (Academic Press, 1966).
16. Curtin Matheson Scientific Inc. Glass type: Erie 2957, Glass Chemical Compositions: 72.6%SiO2, 14.3%NaO, 6.3%CaO, 4.1%MgO, 1.12%Al2O3, 1.16%KO, 0.3%SO3, 0.03%Fe2O3, 0.05%TiO2. Refractive indexes : n(480nm)=1.5213, n(546nm)=1.5170, n(644nm)=1.5120
17. H. M. Milchberg, I. Lyuvbomirsky & C. G. Durfee III. Phys. Rev. Lett. 67, 2654-2657 (1991).
18. P. H. Y. Lee & O. Willi. Laser & Particle Beams 3, 263 (1985).

DATE
FILMED
9/20/93

END